



URANS COMPUTATIONS OF A 3-D SINGLE-PHASE VERTICAL HEATER VERTICAL COOLER NATURAL CIRCULATION LOOP

Constantinos Katsamis^{1*}, Tim J. Craft¹, Hector Iacovides¹, Juan Uribe²

¹Department of Mechanical, Aerospace and Civil Engineering, University of Manchester, M13 9PL, UK

²EDF Energy R&D UK Centre, Manchester, United Kingdom

ABSTRACT

This investigation presents 3D simulations of the flow dynamics and thermal transient behaviour in a rectangular Natural Circulation Loop (NCL) system for nuclear thermal hydraulics purposes. The heating/cooling arrangement consists of vertical heater and cooler on opposite side legs of a rectangular loop at operating conditions that allow the flow to reach a turbulent state. The time-dependent computations are aimed at testing the performance of a number of RANS models, both eddy-viscosity and second-moment closures, using different near-wall treatment and turbulent heat flux models. All the computations include conjugate heat transfer analysis to account for the effects of thermal inertia of the solid material. The effects of 3D flow structures present in the flow are also investigated in the present study.

1. INTRODUCTION

The future of emergency cooling systems in the forthcoming generation IV nuclear reactors is expected to rely mainly on natural circulation, thus contributing towards the simplification, safety, and reliability of the emerging designs [1], [2]. A knowledge gap exists on experimental and numerical studies on related closed cooling systems, with more recent efforts focusing on either rectangular or toroidal loop geometries known as thermosyphons [3, 4]. These configurations can have a variety of heating arrangements by changing the positions of the heater and the cooler. In such devices the temperature differences give rise to buoyancy forces, leading to fluid motion around the loop, thus transporting thermal energy from the high temperature source to the low temperature sink. The fluid motion depends on the balance between the buoyancy forces and the frictional forces on the pipe walls, and the heating and cooling arrangements can influence whether the system will reach a steady-state or remain chaotic. For example, the Vertical Heater Vertical Cooler (VHVC) configuration, such as that shown on Figure 1, can lead to a fairly stable circulation around the loop, under certain conditions, whereas if the heater and cooler are placed on the bottom and top horizontal legs of the loop then the flow tends to exhibit high levels of unsteadiness and instability [5], [6], [7]. Several experimental and numerical studies have performed 1-D linear stability analysis of NCLs to understand the mode and threshold limit of the instabilities. Amongst the experimental studies, different geometrical parameters, including pipe diameter, loop aspect ratio, different fluids other than water and heater/cooler orientations have been explored to assess their effects on the flow stability. Generalised laws that rely on forced convection correlations have been proposed to predict flow characteristics across laminar, transitional, and turbulent conditions. Computational Fluid Dynamics (CFD) studies on modelling NCLs are not as common, although [8] reported results from different heater/cooler configurations in a rectangular loop, showing agreement with the correlations of [5], in an effort to understand the fluid circulation and flow reversals.

The present work investigates the capabilities of URANS in modelling the rectangular VHVC loop of [4], [6] with a total loop circulation length over the diameter ($N_G = L_t/D$) of 266.4, with water as the fluid ($Pr = \nu/\alpha = 1 - 2.25$). This configuration is reported to reach a steady-state in most previous studies, with a clockwise fluid circulation around the loop. Therefore, the performance of a range of RANS models once the flow has reached a steady-state is assessed in the present study. Different near-wall modelling treatments are also tested, including an advanced wall function treatment (the AWF), to provide some further insight on the effects of turbulence and near-wall heat transfer. The numerical explorations concern single phase flow at two heating powers, $Q = 1.015kW$ for which there is

*Corresponding author: constantinos.katsamis@manchester.ac.uk (Constantinos Katsamis)

experimental data available, and at much higher heating power ($5kW$) which is sufficient to generate significant levels of turbulence. With regards to the heat extraction, the cooler side is maintained at a constant temperature of $T_c = 34^\circ\text{C}$ and all the computations account for heat conduction in the borosilicate pipe walls with thickness of 2mm.

2. FLOW CHARACTERISATION AND CFD MODELLING

The flow regime is characterised by the proposed modified Grashof number that arises from the 1-D form of the transport equations according to [5]:

$$Gr_m = (D_h^3 \rho^2 Q \Delta H_c \beta g) / (A \mu^3 c_p) \quad (1)$$

where D_h stands for the pipe hydraulic diameter, ΔH_c denotes the height of the loop, ρ the fluid density, c_p the specific heat capacity, μ the dynamic viscosity, A the cross-sectional flow area, g the gravitational acceleration and β the volumetric expansion coefficient.

For the VHVC configuration many experiments have measured the temperature difference (ΔT_h) along the heated section of the loop and used this to estimate the mass flow rate around the loop (assuming the energy balance at steady-state, $\dot{m}_Q = Q / c_p \Delta T_h$). Correlations have then been developed linking the Reynolds number under these steady-state conditions (Re_{ss}) to Gr_m , of the form:

$$Re_{ss} = C (Gr_m / N_G)^r \quad (2)$$

with coefficients typically given as $C=0.1768$, $r=0.5$ for laminar flow and $C = 1.96$, $r = 1/2.75$ for fully turbulent cases [6].

The above correlations can allow comparisons with the steady-state experimental data. However, to compare the different models' predictions at different sections of the loop, the predicted quantities are non-dimensionalised using the temperature and velocity scales that arises from the original definition of the Grashof number and the heater area ($A_h = \pi D L_h$), given by:

$$\Delta T_r = Q D / (A_h \mu c_p) \quad (3)$$

$$V_b = \sqrt{g \beta \Delta T_r D} \quad (4)$$

The open source code, *Code_Saturne v5.0.8*, developed by EDF is chosen to solve the unsteady transport equations of mass, momentum and energy using the Finite Volume Method [9]. The convective discretisation is handled using a second-order based upwind scheme for mean quantities and first order for the turbulent variables. The pressure correction algorithm adopted is SIMPLEC and the time discretization follows a 1st order implicit time scheme with a time step of $\Delta t = 0.006s$, achieving a CFL in the order of unity. The contribution of buoyancy in the momentum equation is modelled through the variable fluid properties approach with the properties being evaluated from [10] at a pressure of 10MPa to avoid boiling.

2.1 Turbulence and near-wall modelling

Eddy viscosity models (EVMs), such as the low-Reynolds number *Launder and Sharma* form ($k - \epsilon LS$) [11] and the more advanced closure of [12], an elliptic blending Reynolds Stress transport model (EBRSM) are tested here. EVMs utilise an eddy-viscosity, $\nu_t (\propto c_\mu k^2 / \epsilon)$ in order to linearly relate the Reynolds stresses ($\overline{u'_i u'_j}$) that arise from Reynolds-averaging with the mean strain rates (assuming the Boussinesq hypothesis) whereas the more elaborate EBRSM solves a transport equation for each of the 6 components of $\overline{u'_i u'_j}$, one for the dissipation rate and one equation for the blending parameter α . For the low-Re models, the viscous sublayer is fully resolved with a grid of 3.062×10^6 control volumes

satisfying $y^+ < 1$ for the near-wall node. The high-Re $k - \varepsilon$ form of [13] with the standard log-law based wall function (SWF) is also assessed here which inherits the same number of nodes along the centreline as the low-Re mesh and a coarser near-wall grid with a total of 0.912×10^6 ($y^+ > 24$).

In buoyancy-driven flows the steep near-wall gradients do not obey the logarithmic law of the wall, which makes them particularly challenging to model with a log-law based wall function treatment. Thus, a new variant of the Analytical Wall Function (AWF) of [14] has been introduced and tested for the natural circulation flow within the loop (refer to [15] for further information). The approach accounts for the near-wall eddy viscosity variation, convective transport, and buoyancy effects by solving a simplified momentum equation of the form:

$$\frac{\partial}{\partial y} \left[(\mu + \mu_t) \frac{\partial U}{\partial y} \right] = \frac{\partial U}{\partial x} - \frac{\partial P}{\partial x} + \rho g_x \quad (5)$$

The simplified temperature equation follows a similar form of equation (5), and the new approach performs the integration numerically by fitting a near-wall sub-grid instead of adopting the analytical expressions derived in the original proposal. The numerical solution of the sub-grid temperature and velocity is used to approximate the wall heat flux, shear stress and contributions to the turbulent equations. Regarding, the turbulent heat flux modelling, the effective diffusivity approach is used alongside the EVMs, whereas the Generalised Gradient Diffusion Hypothesis is applied with the EBRSM.

3. RESULTS AND DISCUSSION

The simulations of the VHVC arrangement confirmed that the flow reaches a steady-state, following a clockwise motion around the loop, in agreement with previous experimental studies. Evidence of this is exhibited from time histories of the computed mass flow rate ($\dot{m}_{ss} = \int \rho \vec{U} \vec{n} dA$) across a section of the loop from the two different heating powers using the $k - \varepsilon$ LS, where no change in sign is observed (Figure 1(b)). Considering the effects of the heat conduction in the pipe walls caused a damping of the oscillations of the mass flow rate, suggesting that the thermal inertia has a strong influence on the heating and cooling process. Increasing the heating power by a factor of five led to about 3 times greater \dot{m}_{ss} . It is worth noting here that the low-Re models tended to laminarize the flow before it could develop into a fully turbulent state at this higher heating power. To overcome this the turbulence was re-initialised during the simulation, by imposing a non-negligible turbulence intensity and ν_t/ν ratio, after which a fully turbulent state could be established. This re-initialisation causes the sudden increase in mass flow rate seen in Figure 1(b). After sufficient time the flow reaches a statistically steady-state in which the heat extracted by the cooler is equal to the fixed heating rate imposed by the heater. The high-Re approaches did not need this re-initialisation treatment, and returned a fully turbulent flow in the higher heating power case.

The steady-state results from all the models are compared to the correlation of equations (1)-(2) proposed by [5] (Figure 2) and further details are provided in Table 1. The predictions of $k - \varepsilon$ LS at $Q = 1.015kW$ are seen to agree reasonably well with the experimental values of Gr_m , Re_{ss} , temperature difference across the heater (ΔT_h) and the mean loop temperature, T_{mean} (see Table 1), and the correlation point at this heating rate lies on the lower side of the turbulent regime. For the 5kW case the predictions from all the models agree well with the much higher Re_{ss} of the experiments. Although, all the models' predictions lie close to the correlation lines they are not exactly on them, as the correlations have been developed by making use of global energy, mass and momentum conservation, but not accounting for the effects of near-wall turbulence, 3D non-uniformities and flow structures in the pipe. The computed mass flow rate using the energy balance from all the models is quite similar according to Table 1, and increases by a factor of around 1.6 as the heater power is increased from 1 to 5kW. Table 1 also presents comparisons of the predicted cooler side average Nusselt number, estimated based on the fluid temperature across the cooler and its area, $Nu_c = QD / \lambda A_c (T_w - T_f)$. The EBRSM returns the highest Nu number levels, consisted with the fact that it also returned the highest turbulence levels in the cooler leg. Higher Nu_c number promotes stability of the flow, as the cooler is more effective at

removing heat due to the stronger turbulent mixing. The returned Nu_c from the $k - \varepsilon$ AWF is quite close to that of the EBRSM, whereas the $k - \varepsilon$ LS predicts the lowest Nu_c , followed by the SWF strategy. This suggests that the latter two models returned lower turbulence mixing in the cooler compared to the EBRSM and the $k - \varepsilon$ AWF approaches. Although not presented here, it is also worth noting that the $k - \varepsilon$ SWF model did not reproduce the mixture of laminar and turbulent flow regions being convected around the loop, to the same extent as the low-Re models did.

Time-averaged profiles of temperature and velocity across the outlet of both thermally active sections are included in Figures 3-4. In both thermally active sections the $k - \varepsilon$ LS model returns a nearly symmetric time-averaged temperature profile, with levels much higher compared to those of the EBRSM, which returned the lowest temperatures. The two wall function models return quite similar temperature profiles across both sections. For the dynamic field, all the models return similar vertical velocity levels, as might be expected from the quite similar mass flow rates reported earlier. Overall, a general asymmetry is observed in the velocity profiles across both sections.

Further investigation along the cooling leg of the loop, where the flow cools down as it descends, shows secondary flow patterns at the outlet of the top right elbow, near the cooler inlet. The vortex structure captured using the $k - \varepsilon$ LS, also predicted by the other models, is presented from iso-surfaces of the Q-criterion coloured by the velocity magnitude in Figure 5. Such 3-D flow features occur due to the pressure distribution around all four bends of the loop. The significance of these in relation to the cooler location is highlighted here as, for example, placing the cooler closer to the bend may cause the flow structures to elongate (as the near-wall fluid is accelerated downwards), leading to greater levels of near-wall swirl. This flow feature is quite important in its own right for cooling loops of reactors and suggests that further research is required to determine parameters that can be influential on the loop performance.

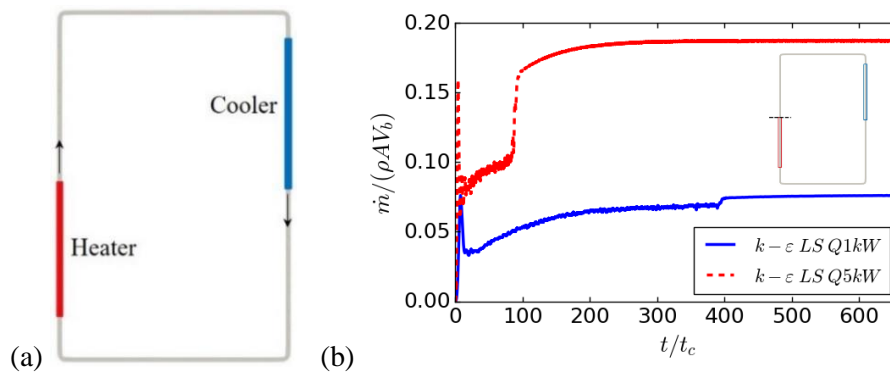


Figure 1: (a) Schematic of the BARC Natural Circulation Loop configuration with VHVC. (b) Time histories of the mass flow rate across the heater outlet at different imposed powers $Q = 1 \text{ kW}$ and 5 kW .

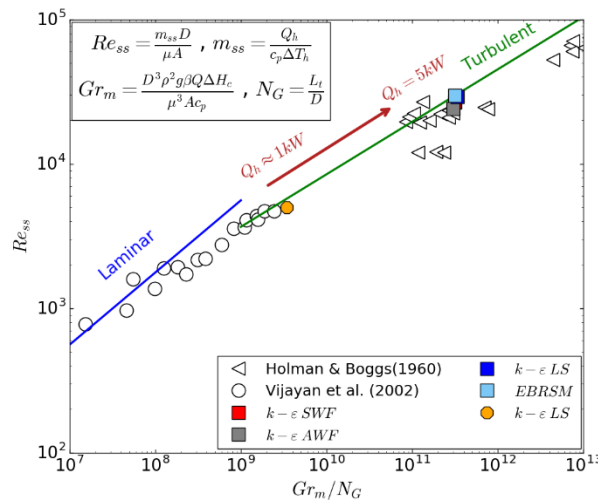


Figure 2: Correlation plot for the different operating conditions.

Table 1: Steady-state characteristics for BARC NCL.

Case	ΔT_h	T_{mean} [K]	\dot{m}_Q [kg/s]	Gr_m/N_G [$\times 10^{11}$]	Re_{ss}	Nu_c
$Q = 5kW$						
$k - \varepsilon$ SWF	11.32	452.55	0.101	3.17	26776	22.79
$k - \varepsilon$ AWF	12.44	448.00	0.093	3.00	24011	24.01
$k - \varepsilon$ LS	10.54	455.17	0.109	3.36	29162	20.81
EBRSM	10.19	450.93	0.113	3.17	29746	25.02
$Q = 1kW$						
$k - \varepsilon$ LS	5.92	345.66	0.043	0.0343	5007	16.32
Exp.	6.54	345.53	0.0374	0.0266	4574	-

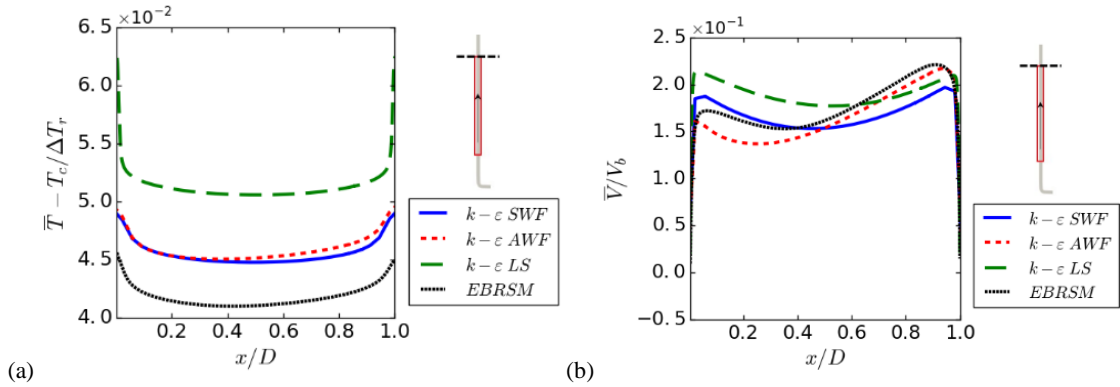


Figure 3: Non-dimensional time-averaged (a) temperature and (b) vertical velocity profiles across the heater outlet.

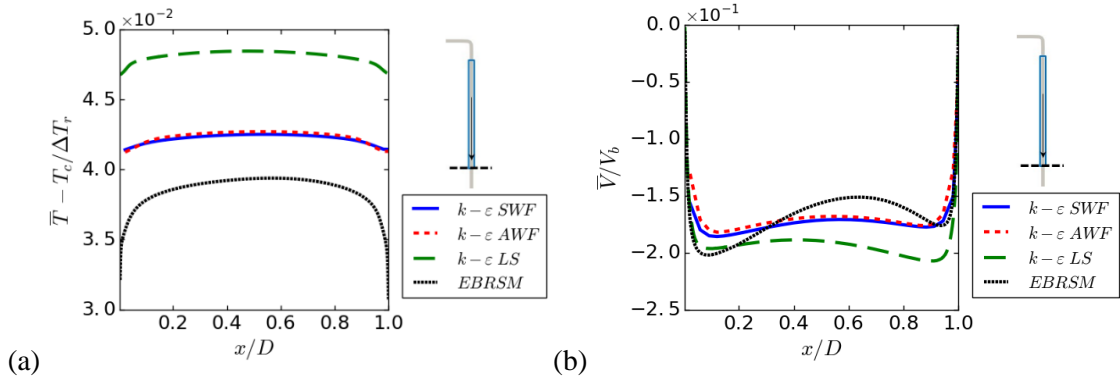


Figure 4: Non-dimensional time-averaged (a) temperature and (b) vertical velocity profile across the cooler outlet.

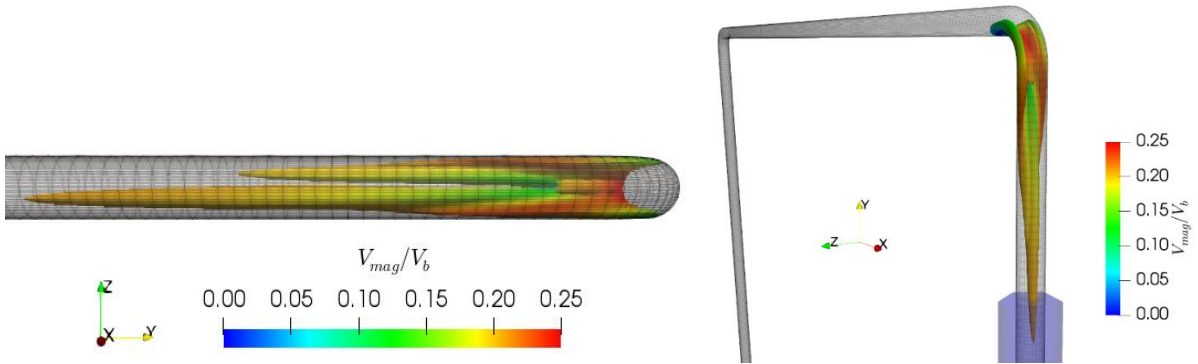


Figure 5: Instantaneous iso-surface Q-criterion coloured with dimensionless velocity magnitude along the cooler side from the predictions of the $k - \varepsilon$ LS in the 3-D BARC NCL.

4. CONCLUSIONS

Transient 3-D RANS computations of the flow in a rectangular NCL have been performed and different models have been compared. The stable behaviour of the VHVC loop at different operating conditions has shown clockwise circulation, as also found in the experimental studies, and the results show generally good agreement with the experimental correlations and estimated \dot{m}_{ss} around the loop. The returned near-wall heat transfer exhibits some variations, with the recently developed AWF approach returning results that are close to the more computationally demanding EBRSM. The AWF has been proved a valuable tool in modelling these flows which require large grid requirements, being highly competitive to the low-Re forms which need very fine near-wall grids, and some specific numeric treatments, to return the correct turbulent behaviour. An investigation of the 3-D effects revealed secondary motion at the four elbows of the loop. The vortex structure developed needs to be further investigated since geometrical parameters such as the cooler location may influence its elongation and further LES or even DNS computations of VHVC NCLs are recommended.

ACKNOWLEDGEMENTS

The author would like to acknowledge the funding of MACE Beacon Scholarship of The University of Manchester and EDF Energy. The assistance given by Research IT, and the use of The HPC Pool funded by the Research Lifecycle Programme at The University of Manchester are also acknowledged.

REFERENCES

- [1] IAEA, Natural Circulation in Water Cooled Nuclear Power Plants. (*No IAEA-TECDOC-1474*), (2005).
- [2] IAEA. Progress in the methodologies for the assessment of passive safety system reliability in advanced reactors: results from the coordinated research project on development of advanced methodologies for the assessment of passive safety systems performance in advanced reactors. (*No. IAEA-TECDOC-1752*), (2014).
- [3] E. Merzari, P. Fisher, W. D. Pointer, Optimal Disturbances in three-dimensional natural convection flows. *Proceedings of the ASME Fluids Engineering Summer Meeting, FEDSM2012*, (2012).
- [4] Vijayan, P. K., Bhojwani, V. K., Bade, M. H., Sharma, M., Nayak, A. K., Saha, D., and Sinha, R. K., Investigations on the Effect of Heater and Cooler Orientation on the steady state, transient and stability behaviour of single-phase natural circulation in a rectangular loop. (*No BARC –2001/E/034*), Bhabha Atomic Research Centre Mumbai, India (2001).
- [5] Vijayan, P. K., Experimental observations on the general trends of the steady state and stability behaviour of single-phase natural circulation loops. *Nuclear Engineering and Design*, **215** (1) (2002), 139–152.
- [6] Vijayan, P. K., Sharma, M., and Saha, D., Steady State and Stability Characteristics of Single Phase Natural Circulation in a Rectangular Loop with Different Heater and Cooler Orientations. *Experimental Thermal and Fluid Science*, 31(8), (2007) 925–945.
- [7] J. P. Holman and H. Boggs, Heat Transfer to Freon 12 Near the Critical State in a Natural-Circulation loop, *In. J. of Heat Transfer* 82(3) (1960) 221-226.
- [8] J. Kudariyawar, A. Vaidya, N. Maheshwari, Computational study of instabilities in a rectangular natural circulation loop using 3D CFD simulation. *In. J. of Thermal Sciences*, **101** (2016) 193–206.
- [9] Archambeau F., Méchitoua N., and Sakiz M., Code Saturne: A Finite Volume Code for the computation of turbulent incompressible flows– Industrial Applications. *In. J. on Finite Volumes* **1** (2004) 1-62.
- [10] IAPWS (2007). Revised Release on the IAPWS Industrial Formulation 1997 for the Thermodynamic Properties of Water and Steam. *Technical report*. <http://www.iapws.org/relguide/IF97-Rev.html>.
- [11] Launder, B. E. and Sharma, B. I., Application of the energy-dissipation model of turbulence to the calculation of flow near a spinning disc. *Letters in Heat and Mass Transfer*, **1** (2) (1974) 131-137.
- [12] Manceau R., Recent progress in the development of the Elliptic Blending Reynolds-Stress model, *In. of Heat and Fluid Flow*, **51** (2015) 195-220.
- [13] Launder, B. E. and Spalding, D., The numerical computation of turbulent flows. *Computer Methods in Applied Mechanics and Engineering*, **3** (2) (1974) 269-289.
- [14] Craft T. J., Gerasimov A. V., Iacovides H., & Launder B. E., Progress in the generalization of wall-function treatments. *In. J. Heat and Fluid Flow*, **23** (2002) 148–160.
- [15] Katsamis, C., Craft, T., Iacovides, H. and Uribe, J., “Use of 2-D and 3-D unsteady RANS in the computation of wall bounded buoyant flows”. *Int. J. Heat and Fluid Flow*, **93** (2022)108914.